Energy & Environmental Science

PAPER

View Article Online
View Journal | View Issue

Cite this: *Energy Environ. Sci.*, 2015, **8**, 2118

Defect migration in methylammonium lead iodide and its role in perovskite solar cell operation†

Jon M. Azpiroz,[ab] Edoardo Mosconi,*[a] Juan Bisquert[cd] and Filippo De Angelis*[a]

In spite of the unprecedented advance of organohalide lead perovskites in the photovoltaics scenario, many of the characteristics of this class of materials, including their slow photoconductivity response, solar cell hysteresis, and switchable photocurrent, remain poorly understood. Many experimental hints point to defect migration as a plausible mechanism underlying these anomalous properties. By means of state-of-the-art first-principles computational analyses carried out on the tetragonal $MAPbI_3$ (MA = methylammonium) perovskite and on its interface with TiO_2, we demonstrate that iodine vacancies and interstitials may easily diffuse across the perovskite crystal, with migration activation energies as low as ~0.1 eV. Under working conditions, iodine-related defects are predicted to migrate at the electrodes on very short time scales (<1 μs). MA and Pb vacancies, with calculated activation barriers of ~0.5 and 0.8 eV, respectively, could be responsible for the slow response inherent to perovskites, with typical calculated migration times of the order of tens of ms to minutes. By investigating realistic models of the perovskite/TiO_2 interface we show that negatively charged defects, *e.g.* MA vacancies, close to the electron transport layer (TiO_2 in our case) modify the perovskite electronic state landscape, hampering charge extraction at selective contacts, thus possibly contributing to the observed solar cell hysteresis. We further demonstrate the role of the electron transport layer in affecting the initial concentration of defects close to the selective contacts, highlighting how charge separation at the perovskite/TiO_2 interface may further change the defect distribution. We believe that this work, identifying the mobile species in perovskite solar cells, their migration across the perovskite material, and their effect on the operational mechanism of the device, may pave the way for the development of new materials and solar cell architectures with improved and stabilized efficiencies.

Received 23rd April 2015,
Accepted 28th May 2015

DOI: 10.1039/c5ee01265a

www.rsc.org/ees

Broader context

Hybrid lead-halide perovskites have revolutionized the scenario of emerging photovoltaic technologies, thanks to their unique set of properties. Since the seminal work by Kojima *et al.* in 2009, perovskite solar cells (PSCs) have experienced an exponential growth, with photovoltaic efficiencies now topping 20%. In spite of such an impressive development, an in-depth understanding of many of the physical properties of this class of eclectic materials remain elusive, including ion (defect) migration, which could explain the slow photoresponse, the *J–V* hysteresis, and the switchable photovoltaic effect. Based on first-principles simulations, we identify iodide vacancies and interstitials as the most mobile defects, followed by methylammonium vacancies and lead vacancies, which have increased activation energies. The accumulation of defects close to the selective contacts under operative solar cell conditions is predicted to modify the landscape of the perovskite electronic levels, hampering charge separation and presumably lowering the performance of the device. This work, identifying the mobile defects in PSCs, their migration across the perovskite material, and their effect on the operational mechanism of the device, may provide a basis for the interpretative framework required for the development of new materials and device architectures with enhanced functionality.

[a] *Computational Laboratory for Hybrid/Organic Photovoltaics (CLHYO), Istituto CNR di Scienze e Tecnologie Molecolari (ISTM-CNR), Via Elce di Sotto 8, 06123, Perugia, Italy. E-mail: edoardo@thch.unipg.it, filippo@thch.unipg.it*
[b] *Kimika Fakultatea, Euskal Herriko Unibertsitatea (UPV/EHU), and Donostia International Physics Center (DIPC), P. K. 1072, 20080 Donostia, Euskadi, Spain*
[c] *Institute of Advanced Materials (INAM), Universitat Jaume I, Castello de la Plana, Spain*
[d] *Department of Chemistry, Faculty of Science, King Abdulaziz University, Jeddah, Saudi Arabia*

† Electronic supplementary information (ESI) available. See DOI: 10.1039/c5ee01265a.

1. Introduction

Since the pioneering work by Kojima *et al.*,[1] organohalide lead perovskites have revolutionized the field of emerging photovoltaic technologies. By changing the electrolyte formulation and the deposition method of the perovskite sensitizer on TiO_2, Park *et al.* were able to improve the power conversion efficiency (PCE) from the original 3.8% by Kojima *et al.* to 6.5%.[2]

Replacing the liquid electrolyte with a solid-state hole conductor represented another step forward both in terms of stability and efficiency, reaching PCE values of 9.7%[3] and 10.2%.[4] Lee *et al.* demonstrated that substituting the TiO_2 substrate with a mesoporous scaffold made of Al_2O_3 produced similar conversion efficiencies, suggesting that the perovskite itself works as an electron transporter.[4] At the same time, Etgar *et al.* showed that the perovskite could also assume the role of a hole transporter material,[5] which prompted the development of new device architectures. Over the last three years, perovskite solar cells (PSCs) have experienced an unprecedented development,[6–8] with various reports of efficiency close to 20%,[9,10] and a certified 20.1% efficiency value.

In spite of such a ''perovskite storm'', many of the properties of this class of eclectic materials remain elusive. In particular, there are three unusual findings that have earned a lot of attention, namely (i) the slow electrical material response under light irradiation;[11,12] (ii) the anomalous hysteresis of the current–voltage (*J–V*) curves shown by various PSC devices;[13–18] and (iii) a recently reported giant switchable photovoltaic effect.[19,20]

In the former case, measurements by Gottesman *et al.* showed a slow (seconds to minutes) conductivity response of the methylammonium lead iodide ($MAPbI_3$) perovskite under illumination.[11] A possibly related phenomenon was reported by Sanchez *et al.*, who found a giant photoinduced dielectric constant in $MAPbX_3$ perovskites (X = I, Br, Cl).[12] Regarding the hysteresis, the *J–V* behavior of PSCs is known to strongly depend on the employed electron transport layer (*e.g.* organics, Al_2O_3 or flat/mesoporous TiO_2).[13–17] Moreover, the operational point preceding the measurement (*i.e.* dark, open-circuit, or short circuit) strongly modulates the shape of the *J–V* curve. Furthermore, the J-scanning sweep rate strongly affects the shape of the *J–V* curves in various types of devices.[13–15] Adding to this discussion, a very recent paper by Xiao *et al.* reported a giant switchable photovoltaic effect, which was observed after poling with an external electric field, on a $MAPbI_3$-based device built with non-selective contacts.[19,20]

The slow photoinduced response, the hysteresis and the switchable photovoltaic effect could be different macroscopic manifestations of a possibly similar underlying microscopic picture. Some experimental results pointed to the role of interface effects as the origin of these anomalous phenomena.[15] The slow photoconductivity or dielectric response and hysteresis are observed for a variety of device architectures (on Al_2O_3, TiO_2, and with or without hole transport layer), and even with different perovskites (*e.g.* mixed halides *vs.* purely iodide), which turns the focus to possible general properties of organohalide perovskites.[15] Notably a sizable dependence of the *J–V* hysteresis on the nature of the electron transport/collection layer has also been observed, with devices employing a flat TiO_2 layer showing increased hysteresis compared to those based on a mesoporous TiO_2 scaffold.[14,17] Employing fullerene derivatives as an electron transport/collection layer was also shown to reduce the PSC hysteresis.[21–24] These observations call for an interplay of interfacial and intrinsic perovskite properties as the reasons underlying the *J–V* hysteresis in PSCs. In particular, on mesoporous TiO_2 a highly efficient interfacial electron transfer was found,[25] while a barrier at the flat perovskite/TiO_2 interface was recently proposed.[24] Such a barrier was not found at the perovskite/C_{60} interface, suggesting that efficient electron extraction may be the route to less severe *J–V* hysteresis. This analysis does not explain, however, the dependence of the *J–V* curve on the scan rate in mesoporous TiO_2-based devices.[14,15]

Among the various hypotheses that have been put forward to explain the characteristics of PSCs, the most commonly invoked ones are: (i) charge trapping;[21–23,26] (ii) ferroelectricity;[11,27–30] and (iii) ion/defect migration or conductivity.[17,20]

Regarding charge trapping, organohalide perovskites are prone to defect formation, due to the low thermal stability of the material.[21] Imperfections on the perovskite surface and at grain boundaries may introduce localized states, which could capture photogenerated carriers and therefore induce a field across the material that would eventually counteract the photogenerated potential. C_{60} fullerenes deposited on the perovskite surface may prevent the appearance of defect states, eliminate the photocurrent hysteresis, and double the conversion efficiency of the solar device.[21,23] Trap states are not limited to the perovskite material, but they can also affect other components of the solar device. Nagaoka *et al.* reported that doping the TiO_2 substrate with Zr and passivating the surface with pyridine molecules mitigate the defect state density in the oxide, which in turn increases the power conversion efficiency and reduces the hysteresis.[26] Snaith and coworkers proposed an elegant modification of the perovskite/TiO_2 heterojunction, which is based on the incorporation of a self-assembled monolayer of functionalized C_{60} fullerenes.[22] The C_{60} monolayer should hinder the development of trap states at the interface with the oxide through a carboxylic anchoring group, and on the perovskite side by means of the pending fullerene moiety. Furthermore, it has been very recently proposed that fullerene may interact with halide-rich defective regions at the grain boundaries of $MAPbI_3$, leading to a passivation of the related trap states and diminishing the hysteresis of the associated PSCs.[31] The role of the C_{60} monolayer is not limited to the appearance of trap states, but it may also induce n-doping of the perovskite edge in contact with the TiO_2 substrate, which in turn triggers the interfacial electron transfer.[22] In addition, a very recent work by Xing *et al.* has proposed that interfacial dipoles originating from defect compensation at the perovskite/TiO_2 interface could be related to *J–V* hysteresis; this effect is absent in the case of a fullerene electron transport/collection layer.[24] These results are consistent with those of ref. 22, showing that passivation of defects in TiO_2 was the key to mitigate the hysteresis. Polarization effects in the bulk perovskite could also explain the anomalous properties of PSCs. Recent experimental studies have shown the presence of sizable ($\sim$100 nm size) ferroelectric domains in $MAPbI_3$ thin films.[29] These domains are characterized by a permanent polarization, which would eventually compensate the photogenerated field. Three mechanisms could explain such a polarization, *i.e.* ionic off-centering, atomic PbX_6 octahedra rotation, and organic cation dipolar orientation.[27] The latter seems to be the most

likely hypothesis, as supported by theoretical calculations.[28,30] However, the rotation of the polar MA molecules is extremely fast and cannot alone account for the slow response phenomena observed in organohalide perovskites, while the rearrangement of the inorganic scaffold, which follows the reorientation of molecular dipoles, could be responsible for the experimental findings.[11] Furthermore, a recent estimate for the polarization of $MAPbI_3$ of 4.4 $\mu C\ cm^{-2}$ was reported, related to a structure which is only about 0.02 eV per formula unit below a non-ferroelectric disordered structure.[32] It is thus likely that at room temperature the material will not exhibit macroscopic spontaneous polarization. This is also confirmed by ref. 20 in which a lateral device did not show the typical voltage increase observed in photoferroic devices and recent measurements by Coll *et al.* and by Beilsten-Edmands *et al.* indicated that $MAPbI_3$ does not exhibit permanent polarization at room temperature.[33,34]

Recent work by Tress *et al.* has critically assessed the role of charge trapping and ferroelectricity as the source of the slow response and hysteresis.[15] Charge trapping is supposed to occur on much faster timescales than those observed experimentally, while these authors proposed that ferroelectric nanodomains would unlikely influence the solar cell photocurrent. Therefore, while the role of the cation orientation in determining the slow electrical response and possibly the solar cell hysteresis is still a matter of debate, ion or defect migration seems to plausibly contribute to the particularities of organohalide perovskites. Since this is likely an intrinsic property of the perovskite, however, ion/defect migration alone cannot explain the role of interfacial phenomena in determining the hysteresis and again call for an interplay of these two factors. Recent work by O'Regan *et al.* has also shown the existence of two types of extractable charges stored in PSCs, with the slower component associated with dipole realignment or the effect of mobile ions.[35] Beilsten-Edmands *et al.* have also provided further evidence of the importance of ionic migration in modifying the efficiency of PSCs.[34]

Ion or defect migration could also explain the giant switchable photovoltaic effect recently reported by Xiao *et al.*,[19,20] who demonstrated that the photocurrent direction in PSCs may be switched by poling through an applied electric field. This finding reveals the reversible formation of p–i–n junctions at otherwise non-selective contacts, induced probably by ion or defect drifting along the perovskite layer under the influence of an electric field. Ionic transport is indeed well documented for perovskite oxides[36–39] and metal halides.[40] In the former case, ABO_3 (A = La, Sr; B = Mn, Fe, Co, Cr) materials are known for their ionic conductivity, which proceeds by means of a defect-mediated hopping mechanism.[37] Therefore, imperfections in the crystal (mainly ion vacancies and interstitials) are crucial for the process, since ion diffusion is otherwise hard to imagine in a perfect crystal. Theoretical calculations have shown that formation of interstitial defects is very unfavorable in ABO_3 perovskites,[36] which leaves the vacancy-mediated path as the most plausible mechanism for ionic conductivity. Attending to the formation energies, cation vacancies could assist the ion drift along the crystal. However, the huge energy penalties to be surmounted along the migration path, which could amount to 3–4 eV in the case of La, hinder cation diffusion in perovskite oxides.[36] Therefore, oxygen vacancies are assumed to be the lowest energy path for ionic migration in ABO_3 perovskites.[38,39] Organohalide lead perovskites, with their propensity for defect formation, are potential candidates for ionic conductivity, as pointed out by Dualeh *et al.*[17] This observation could be related to the work of Hoke *et al.*, who found that under light irradiation a mixed halide $MAPbI_{3-x}Br_x$ perovskite evolved into two I-rich and Br-rich partly segregated phases.[41]

Despite various reports now pointing at ion or defect migration as a possible cause for the particular properties of perovskites, the identification of the migrating species and a quantitative understanding of the underlying energetics are still lacking. Here we report state-of-the-art first principles computational analyses on realistic models of $MAPbI_3$ and $MAPbBr_3$ along with the crucial $MAPbI_3$ interface with TiO_2. Building on previous theoretical studies which identified the most probable defects occurring in $MAPbI_3$,[42–46] we evaluate their migration energetics in tetragonal supercells. We find that both iodine vacancies interstitials show a very low activation energy to migration, $\sim$0.1 eV, followed in the order of increasing activation energy by migration of MA ($\sim$0.5 eV) and Pb ($\sim$0.8 eV) vacancies. According to our calculations, the migration of iodine defects seems too fast to produce the slow response typical in $MAPbI_3$ materials, which could better be explained by the diffusion of MA or Pb vacancies. While our models account neither for the combined effect of grain boundaries/amorphous phases and defects in determining the properties of organohalide perovskites nor the difference between *e.g.* flat TiO_2 and C_{60} electron transport layers, and cannot clearly discriminate between mesoporous and flat TiO_2, they are still sufficiently accurate to disclose the preferential location of defects close to the perovskite/TiO_2 interface (be it mesoporous or flat), and allow us to set up a quantitative model explaining the effect of migrating defects in operative solar cell architectures.

2. Results and discussion

Previous computational studies[42–46] have highlighted the defect formation energies for several point defects under various conditions, including vacancies (V_{MA}, V_{Pb}, and V_I), interstitials (MA_i, Pb_i, and I_i), cation substitutions (MA_{Pb} and Pb_{MA}), and antisite substitutions (MA_I, Pb_I, I_{MA}, and I_{Pb}). The investigated antisites are predicted to be unstable both energetically and kinetically, so they should spontaneously split into the respective interstitials and vacancies.[44] Vacancies and interstitials are thus the most likely defects, due to their low formation energies, although in general, they create shallow electronic levels close to the band edges, and therefore are predicted not to hamper carrier transport across the device.[46] According to previous studies,[43,46] under I-poor conditions the material should mainly develop iodine vacancies, V_I, while under I-rich conditions, MA and Pb vacancies (V_{MA} and V_{Pb}) and iodine interstitials (I_i) should be the most likely defects. In this work

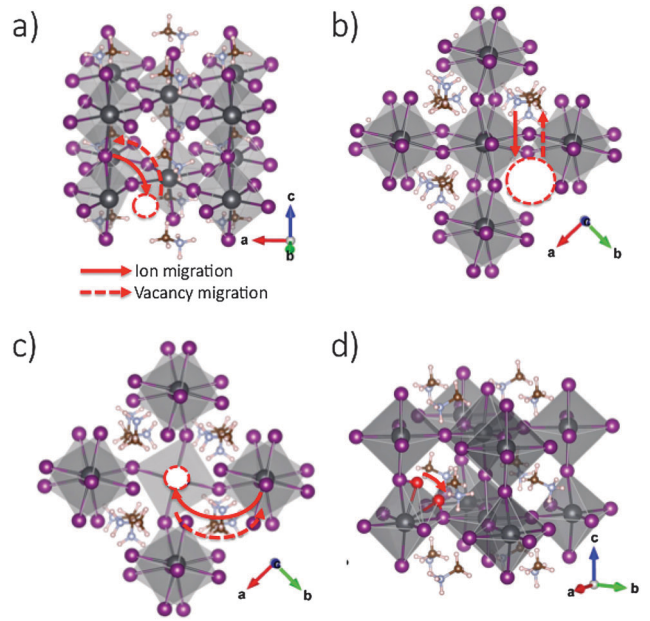

Fig. 1 Diffusion paths for the V_I (a), V_{MA}, (b), V_{Pb} (c) and I_i defects (d). For I_i, the initial and the final configurations are shown. Vacancies are highlighted with dashed circles. Red atoms refer to interstitial defects. Solid lines stand for the migration of the ions, whereas dashed lines indicate the trajectory of the vacancy. White = H, brown = C, blue = N, purple = I, and black = Pb atoms.

we have thus focused on these four defects, and evaluated their possible diffusion pathways and energetics in $MAPbI_3$. To do so, we have built up a simulation cell containing 32 $MAPbI_3$ units (384 atoms),[32] large enough to accommodate the point defects considered and their diffusion, see Models and computational details and ESI.† To preliminarily estimate the role of different halides in determining the defect migration energies we also performed selected calculations on $MAPbBr_3$ adopting the same model as for $MAPbI_3$ except for the use of pseudo-cubic cell parameters.

To model defect migration along the perovskite crystal, we have devised a migration path for each of the four investigated defects, Fig. 1, and identified the corresponding saddle point. For V_I, we create the vacancy in an equatorial position and let the vacancy migrate towards an axial site, Fig. 1a. Note that while V_I in axial or equatorial sites is essentially isoenergetic (within less than 0.01 eV), the axial site is favored by 0.07 eV over the equatorial site for V_{Br}, see ESI.† One could also calculate the V_I migration between two equatorial sites, but the activation energy is supposed to remain almost unchanged, as in previous theoretical studies on perovskite oxides.[47] Regarding V_{MA}, we investigate the hopping of the vacancy between adjacent cavities of the inorganic scaffold that lie in the *ab* plane, Fig. 1b. A similar pathway could be devised along the *c* axis, but no changes in the activation energy are expected, as observed for Mg in $MgSiO_3$ perovskites.[47] In fact, both processes imply that V_{MA} migrates across a Pb_4I_4 framework. Similar to V_{MA}, for V_{Pb} an in-plane migration has been initially studied, in which V_{Pb} moves along the side of the square formed by four Pb and four I atoms, Fig. 1c. Following previous theoretical studies on ABO_3 perovskites,[47,48] we have also considered a second migration path for V_{Pb}, which takes place along the diagonal of the aforementioned Pb_4I_4 framework. However, this migration mechanism implies a larger activation energy (1.06 *vs.* 0.80 eV), making this second pathway less likely, see ESI.† Therefore, in the following discussion we will focus our attention on the lowest-energy V_{Pb} migration path. For I_i, a path along the *c* axis has been drawn, Fig. 1d, similar to V_I. In the starting/final configurations, the interstitial I atom inserts between a couple of axial/equatorial iodine atoms, with almost equal distances (3.87 and 3.96 Å, respectively), in line with the results reported by Du.[49]

Note that due to the proposed pathways, we reasonably assign a comparable migration energy to different defects related by the displacement of the same chemical species, *i.e.* those involving diffusion of MA (*e.g.* MA_{Pb} or MA_i) should display similar activation energies as that calculated for V_{MA}. In fact, as shown below, the activation energies of V_I and I_i essentially coincide. Similar arguments hold for $MAPbBr_3$.

In Table 1 the activation energies (E_a) for the different defect migration are summarized. As one may note from Fig. 1, for $MAPbI_3$ the paths for V_{MA} and V_{Pb} migration are twice as long as the ones devised for V_I and I_i. V_{MA} and V_{Pb} will migrate across one unit cell, whereas V_I and I_i would hop along half the cell. Therefore, in order to fairly compare the four processes, we multiply the activation energies calculated for the iodine-related point defects by a factor of two, corresponding to two consecutive hopping events, see ESI.† Based on the calculated activation energies, we are able to provide an estimate for the migration rate by means of the Arrhenius equation:

$$k = \frac{k_B T}{\hbar} e^{-\frac{E_a}{RT}} \quad (1)$$

where k_B stands for the Boltzmann constant, T is the temperature, $\hbar$ is the reduced Planck constant, and R is the ideal gas constant.

From Table 1 it appears that in $MAPbI_3$ migration of V_{Pb} is quite a slow process, due to its high activation energy, which stands at 0.80 eV, and the consequently low migration rate ($1.2\ s^{-1}$). The diffusion of V_{MA} is characterized by an energy barrier of 0.46 eV, in excellent agreement with the activation energy experimentally found by Almora *et al.* for electrode polarization in PSCs, which amounts to 0.45 eV.[50] According to eqn (1), the calculated activation energy value should deliver a migration

Table 1 Activation energies (E_a, in eV) and rate constants (k, in s^{-1}), calculated according to eqn (1), for the migration of the different investigated point defects in $MAPbI_3$ and $MAPbBr_3$. Values in parentheses for $MAPbI_3$ refer to the energetics and rates of two consecutive hops

	$MAPbI_3$		$MAPbBr_3$	
Defect	E_a (eV)	k (s^{-1})	E_a (eV)	k (s^{-1})
$V_{I/Br}$	0.08 (0.16)	1.7×10^{12} (7.7×10^{10})	0.09	1.2×10^{12}
V_{MA}	0.46	6.5×10^{5}	0.56	1.3×10^{4}
V_{Pb}	0.80	1.2×10^{0}	—	—
I_i	0.08 (0.16)	1.7×10^{12} (7.7×10^{10})	—	—

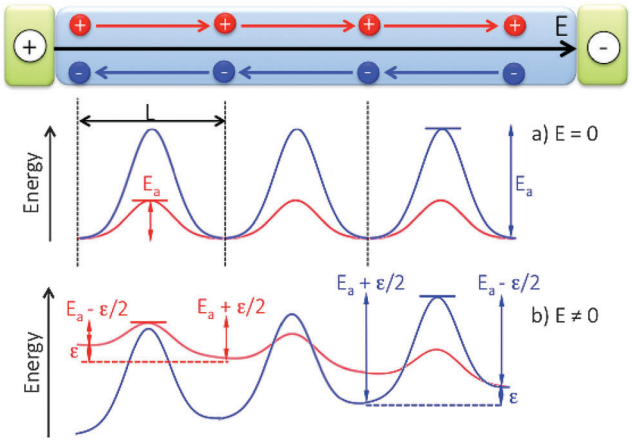

Fig. 2 Sketch of the energy landscape of a positively charged V_I (red) and negatively charged V_{MA} (blue) migration, in the absence of a field ($E = 0$, a) and in the presence of the photogenerated (or external) field ($E \neq 0$, b).

rate of 6.5×10^5 s^{-1} at room temperature. For V_I and I_i we predict a very flat energy pathway, with calculated activation energies of just 0.08 eV, *i.e.* 0.16 eV for a full hop in a given crystallographic direction to take place. Moving to $MAPbBr_3$, a lower total activation energy for a full hop is calculated for V_{Br} compared to V_I, with an asymmetric profile for the former, see ESI,† while a higher value is calculated for migration of V_{MA}, 0.56 *vs.* 0.46 eV. The latter value reflects the reduced lattice dimension of $MAPbBr_3$ compared to $MAPbI_3$, making the passage of MA across two unit cells more difficult in the former.

In the absence of any field, charged defects would follow a random migration path along the perovskite layer. In fact, according to the symmetric energy landscape shown in Fig. 2a, the defect could indistinctly move forward or backward in any given crystallographic direction. In working PSCs, however, the photogenerated field favors migration of the positively/negatively charged defect towards the side of the perovskite film contacting the hole/electron transporting layer (HTL/ETL), respectively. As defects migrate towards the selective contacts, they get stabilized due to the increased electrostatic interaction with the electrode. Such a stabilization, ε, provides the driving force for the migration towards the electrode, lowering the migration activation energy by roughly $\varepsilon/2$ at the transition state, see Fig. 2b for the $MAPbI_3$ case. Similarly, the presence of a field implies an energy penalty of $\sim\varepsilon/2$ for the reverse process, Fig. 2b. For the typical parameters of a working PSC device (the 300 nm thick perovskite layer, and a potential of 1 V), and since in each hop the defect goes across a unit cell of *ca.* 6.5 Å, ε can be estimated to be $\sim$2 meV for a singly (+ or −) charged defect. According to eqn (1), such a small energy penalty implies that the forward hop is roughly 8% faster than the backward step. Note that for defects with the same charge the value of ε is independent of E_a, see also ESI.† For a V_I (or I_i) located in the middle of a 300 nm thick perovskite layer, considering the rate constants in Table 1, the defect would reach the selective contact in tens of ns, much faster than the typical scanning rate employed in photovoltaic measurements. V_{MA}, which we calculate to move more slowly, would reach the ETL in tens of ms, and could therefore affect the *J–V* measurements, possibly explaining the slow response and the hysteresis in current PSCs. V_{Pb} are less mobile and would probably affect the PSC operation on longer time scales (transit time of the order of minutes); although having a −2 charge they are more sensitive to the field than singly charged defects, see ESI.† Notably, higher fields, such as in the presence of an externally applied bias, could further enhance the defect migration in a given direction, reducing the time required to accumulate defects at the selective contacts. The time and field are thus linked variables, in the sense that long times under a weak field may lead to the same effect in terms of defect migration and distribution as short time and strong field. Since the preferential defect migration in a given direction is generated by the (internal or external) field, removing such a field would bring the system back to the original distribution of defects across the perovskite film. This implies that the defects will likely decay in time towards their original (random) distribution, but on a longer time scale compared to the defect migration in the presence of the field. This is consistent with the photocurrent decay of several days observed in poled devices by Xiao *et al.*[20]

In addition to this discussion, it is worth noting that the I-related defects, which are predicted here to reach the selective contacts on very short time scales, will presumably screen the photogenerated field at early times. Such an unbalanced kinetics of defect migration would probably delay the migration of slower-migrating defects, such as V_{MA} or V_{Pb}. At the equilibrium, however, V_{MA} or V_{Pb} defects would likely reach the opposite contacts than the faster-migrating V_I defects, despite an attenuated response due to the screening of V_I.

Moreover, one might wonder if the accumulation of defects close to the selective contacts could induce structural rearrangement of the perovskite material. To simulate this point, we employed a 48 atom tetragonal atom cell, both non-defective and containing V_I in an apical position, and we fully relaxed the atomic and cell parameters of the two systems, see ESI.† Due to the reduced size of the model, this situation corresponds to an upper limit of defect concentration (1/12 defects/iodine atoms). Our calculations reveal a sizable contraction of the unit cell volume ($\sim$11%) due to the halide vacancy. Notably, the system roughly maintains a tetragonal symmetry, with the $c/b \approx a$ ratio only slightly decreasing from 1.486 to 1.451 when passing from the pristine crystal to the defective structure.

Once demonstrated that V_I (or I_i) and V_{MA} are the most mobile species in bulk $MAPbI_3$, we are in a position to judge the impact of their migration on the functioning of PSCs, Fig. 3. Note that the concomitant formation of V_I and V_{MA} was calculated to cost only 0.08 eV by Walsh *et al.*,[45] so we focus here on this combination. Under working conditions the PSC will develop a photogenerated field pointing from the ETL (*e.g.* TiO_2) towards the HTL (*e.g.* Au-coated Spiro-MeO-TAD), Fig. 3a. The photogenerated field will drive V_I migration towards the HTL, while V_{MA} (or I_i) will likely flow in the opposite direction, Fig. 3b. As a consequence, the HTL (ETL) of the PSCs will pile up V_I (V_{MA}), which in turn will create an electrostatic potential

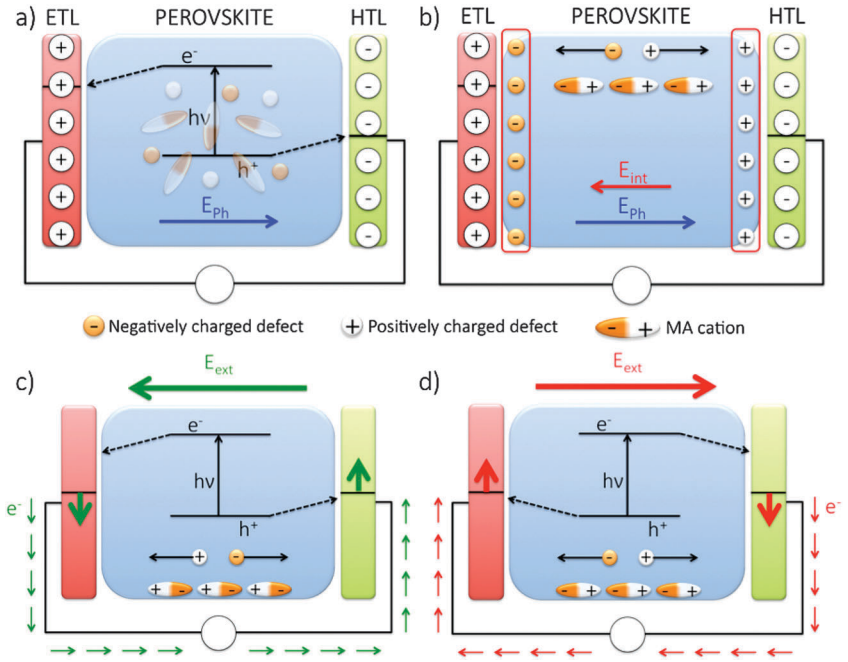

Fig. 3 Sketch of defect migration and their impact on the PSC operational mechanism. (a) shows the separation of the charge carriers driven by the photogenerated potential (E_{Ph}), along with the even distribution of the point defects and the random orientation of the MA cations; (b) depicts the migration of the point defects and the reorientation of the MA cations in response to the photogenerated field (E_{Ph}), and the internal potential developed as a consequence (E_{int}); (c) and (d) show the switchable current as a function of the applied external field (poling).

across the perovskite film, opposite to the photogenerated field that drives charge separation in the solar cell. This internal electric field will eventually hamper transport across the perovskite film and/or charge collection at the electron/hole selective contacts and will ultimately affect the PSC functioning. As one may notice from Fig. 3b, MA cations could also reorient in response to the photogenerated field, therefore contributing to the internal potential generated by the defects piled up at the selective contacts.

The same microscopic mechanism could also explain the hysteresis of the *J–V* curves repeatedly observed in PSCs at different scanning rates. Slowly scanning the device from J_{SC} to V_{OC} would allow defect migration along the perovskite, to partially compensate the photogenerated electric field. On the contrary, starting from V_{OC} or biasing the PSC at V_{OC} before the *J–V* scan would hinder defect migration, and therefore the performance of the device would not be affected. This same picture also explains that, for fast voltage sweep, the measurement is less sensitive to the direction of the scan,[15] since the rate-determining defects have little time to migrate towards the electrodes.

Defect migration may also account for the switchable photovoltaic effect recently found in PSCs.[20] According to Xiao *et al.*,[20] for positive poling, V_I will be gathered at the anode, Fig. 3c. Positively charged defects are predicted to develop shallow states close to the conduction band of the perovskite, leading to n-doping of the perovskite in contact with the anode. Negatively charged ions, in turn, will presumably develop electronic levels above the valence band, inducing p-doping of the perovskite at the cathode. Upon positive poling, Fig. 3c, the PSC behaves as an n–i–p junction, and the current will follow the gradient created along the perovskite upon doping. For negative poling, V_I moves in the opposite direction, giving rise to a p–i–n configuration of the cell and inverting the sense of the current, Fig. 3d.

To provide an atomistic understanding on the mechanism by which defect migration could possibly induce, assist or eventually hamper charge injection and collection across the device, we have calculated the electronic structure of a (110) perovskite slab deposited on top of a (101) anatase TiO_2 substrate,[51] Fig. 4a, as a model of a typically employed electron selective contact, Fig. 3. Note that our TiO_2 model does not include any doping and that the chosen TiO_2 phase and exposed surfaces are those characteristic of the majority of the surfaces exposed to TiO_2 nanoparticles forming the mesoporous film.[52] As discussed above, under working conditions V_I should diffuse towards the HTL-contacting side and V_{MA} towards the ETL side. To simulate this situation, hereafter **1**, we have created V_I at the perovskite surface exposed to the vacuum (*i.e.* to the HTL-contacted surface in a PSC); and a V_{MA} at the oxide-contacting side of the $MAPbI_3$ slab, Fig. 4b. Note that in this model we are considering a V_{MA} defect concentration of 1.6% (*i.e.* one V_{MA} over 60 MA molecues), on the lower edge of what predicted by Walsh *et al.*[45] To model the reverse situation, *i.e.* positive charge accumulation at the $MAPbI_3/TiO_2$ contact, we have then considered a second model, hereafter **2**, which contains V_I at the TiO_2 interface and a V_{MA} at the HTL-contacting side of the perovskite, Fig. 4c. Note that in both **1** and **2** the defects were created without further relaxing the atomic coordinates, to directly assess the impact of such modification on the electronic structure.

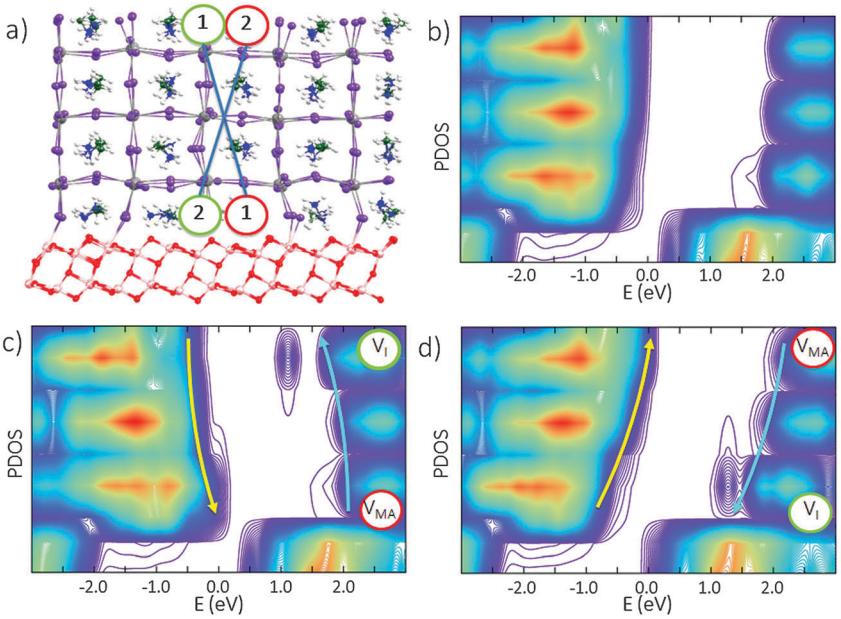

Fig. 4 (a) Model of the perovskite/TiO_2 interface, highlighting the location of V_I (green circles) and V_{MA} (red circles). (b) Local density of states (DOS), projected along the direction orthogonal to the perovskite/TiO_2 interface, for the non-defective model (b), and for the defective cases **1**, (c), and **2**, (d). Light-blue (yellow) arrows are an eye-guide to the evolution of photogenerated electrons (holes).

In Fig. 4, the electronic structure of the defective models **1** and **2** is depicted, along with that of the pristine perovskite/TiO_2 interface. In particular, we analyze the partial Density of States (DOS) partitioned by TiO_2 and $MAPbI_3$ contributions, and its integrated local projection scanned along the direction perpendicular to the TiO_2 surface. As it is evident from Fig. 4b, for the non-defective interface, the outermost valence band (VB) states of the perovskite intrude into the band-gap of the TiO_2 substrate, whereas the unoccupied ones appear to be immersed in the manifold of the conduction states (CBs) of the oxide. This staggered band alignment qualitatively reproduces the energy levels at the perovskite/TiO_2 interface, although with an exaggerated offset between the perovskite and TiO_2 CBs due to the finite size of our system and the inherent inaccuracy of DFT to reproduce the energy levels of semiconductors.[53] A slight bending of the perovskite VB/CB close to the TiO_2 surface is observed, due to the interaction of the material with the substrate.[54] Most notably, the presence of defects has a profound impact on the electronic structure of the perovskite slab and of the overall interface. Irrespective of its localization, V_I creates an unoccupied state *ca.* 0.5 eV below the perovskite CB edge. Note that this value is overestimated compared to previous analyses on the bulk $MAPbI_3$ material, due to the overestimation of the perovskite slab bandgap by *ca.* 0.5 eV. Taking this into account, the state introduced by V_I would basically overlap with the perovskite CB edge, in fair agreement with previous theoretical studies which have assigned V_I as a shallow trap.[43,46] Notably, Du has recently highlighted the importance of spin–orbit coupling and DFT functional in determining the position of the defective levels in $MAPbI_3$.[49] Since in addition to the model limitations we are neglecting these effects in this case, our results on the defect level positioning should be considered as providing only a qualitative overall picture of the defects/interface states.

Importantly, the presence of differently charged defects at the opposite film sides substantially modifies the perovskite VB/CB landscape, this effect being expectedly independent of the level of theory. For system **2**, the presence of V_I close to TiO_2 provides a strong directional gradient of unoccupied states toward the TiO_2 substrate, Fig. 4d, leading to a depletion (accumulation) of unoccupied states in the perovskite bulk (interface). This kind of band bending should definitely assist the separation of photogenerated carriers, funnel electron transport towards the TiO_2 slab, and boost interfacial charge injection. Charge generation is further aided by the MA vacancy in model **2**. In fact, the removal of the organic cation creates a shallow electronic state above the VB edge of the pristine perovskite,[43,46] which further bends the VB. The slope of the occupied states should thus facilitate the diffusion of the photogenerated holes away from the TiO_2 substrate.

Model system **1** delivers a drastically different picture, Fig. 4c. Placing V_I far from the oxide slab inverts the gradient of the band edges, hampering electron injection into the ETL and hole diffusion towards the HTL. This finding clearly demonstrates that the defect migration depicted in Fig. 3b compromises the device performance. At this point, one might wonder if the bending of the band edges could not be overestimated due to the strong electrostatic potential developed between positively charged V_I and negatively charged V_{MA}. We have thus also calculated a modification of models **1** and **2**, which only contain V_I or V_{MA} in the vacuum- and TiO_2-contacting sides of the perovskite and viceversa. The results, see ESI,† show essentially the same VB/CB landscape, although with slightly reduced band bending. Beyond the

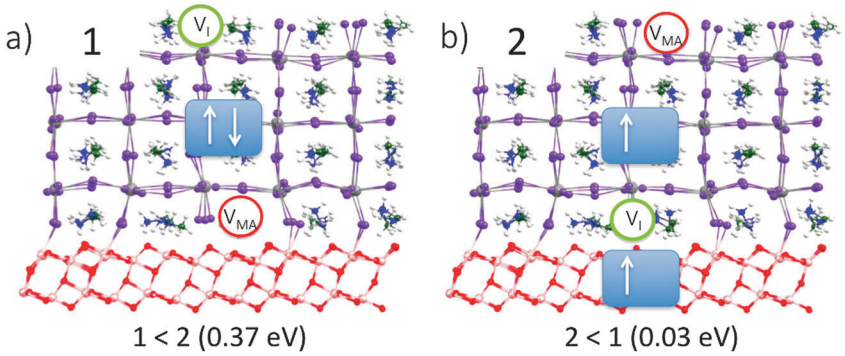

Fig. 5 Preferential location of V_I and V_{MA} in the ground state (a, VB edge localized on the perovskite) and in the charge separated state in which one electron has been promoted from the perovskite to the TiO_2 (b).

aforementioned switchable photovoltaic effect, the overall picture extracted from our calculations nicely matches with the results of Bergmann *et al.*[55] and Edri *et al.*,[56] who reported on the accumulation of holes into the perovskite (and at the perovskite/HTL interface) as a possible explanation of PSC hysteresis.

Furthermore, we propose that in the absence of an electric field anionic defects, such as I_i or V_{MA}, could be preferentially located at the TiO_2 interface since undercoordinated surface Ti(IV) atoms are electron acceptor centers, while positively charged defects may be more evenly distributed across the perovskite film. This is indeed suggested by our non-relaxed calculations providing $\sim$0.4 eV energy stabilization for **1** compared to **2**, which implies a role of the substrate in determining the initial concentration of defects close to the selective contacts.[13] In agreement with our calculations, recent XPS data by Xing *et al.* have highlighted that MA vacancies are preferentially located at the interface with the TiO_2 substrate.[24] It is also plausible that different ETLs from TiO_2 (*e.g.* fullerene derivatives) or the presence of an Au layer in HTL-free devices[57] would change such initial defect distribution. Most notably, by simulating the lowest triplet state of both systems **1** and **2**, in which an electron is promoted from the perovskite VB edge to the TiO_2 CB, Fig. 5, the calculated stability is reversed, with basically no preferential location of V_I and V_{MA}. This situation actually corresponds to a PSC held under open circuit conditions, *i.e.* in which electrons are not extracted from the TiO_2 layer, confirming that under open circuit conditions there is only a limited driving force for defect migration, in line with the reduced hysteresis measured when scanning from V_{OC} to J_{SC}. The landscape of perovskite electronic states remain almost unchanged upon photoexcitation, see ESI.†

3. Conclusions

In summary, we have presented a first-principles computational study, aimed at understanding ion/defect migration in $MAPbI_3$ and $MAPbBr_3$ perovskites, a process that presumably underlies many of the peculiarities of this class of eclectic materials, including slow photoconductivity, hysteresis, and switchable photocurrent. From our calculations, iodine vacancies (interstitials) can easily diffuse along the perovskite crystal, with calculated activation energies of migration of $\sim$0.1 eV. The migration of iodine defects alone is likely too fast to explain the slow (several seconds time scale) response typical in PSCs, although our model does not include the screening effect of such fast-migrating defects on the slower-migrating ones. MA and Pb vacancies, with a calculated activation barrier of $\sim$0.5 and 0.8 eV, respectively, could instead be responsible for this behavior, with typical calculated "response times" of the order of tens of ms to minutes. Most notably, the calculated activation energy value for V_{MA} migration essentially coincides with the experimental activation energy recently reported for electrode polarization in PSCs.[50] Charged defects are predicted to pile up close to the interfaces between the perovskite and the selective contacts. The concomitant field created across the PSC modifies the landscape of the perovskite electronic levels, hampering charge separation and presumably lowering the performance of the device. We believe that this work, identifying the mobile defects in PSCs, their migration across the perovskite material, and their effect on the operational mechanism of the device, may pave the way for the development of new solar cells with improved efficiencies.

Models and computational details

Density functional theory (DFT) calculations have been carried out, within a planewave/pseudopotential approach, as implemented in the PWSCF program of the Quantum Espresso software package.[58] To accommodate the different point defects studied and their migration along the perovskite crystal, a quite large tetragonal unit cell containing 384 atoms (32 PbI_3 units) has been built up.[32] The PBE[59] exchange–correlation functional is used along with ultrasoft, scalar relativistic pseudopotentials for all atoms. Plane wave cutoffs of 25 and 200 Ry are adopted, for expansion of the wave function and density, respectively, sampling the first Brillouin zone at the Γ point only. Electron–ion interactions were described by ultrasoft pseudopotentials with electrons from O, N, and C 2s2p, H 1s, Ti 3s3p3d4s, Pb 6s6p5d, and I 5s5p electrons explicitly included in the calculations. For both geometry optimization and single point calculations we adopted the SR approach. We performed

structural optimizations with cell parameters fixed to the experimental values reported by Poglitsch and Weber.[60] We adopted the scalar relativistic approach (SR), since spin–orbit coupling is known to play a minor role in the structure. Linear transit calculations were performed in order to calculate the energy profile along the migration paths of the defects, identify the saddle point, and estimate the energy barriers. To simulate the perovskite/TiO_2 systems, we optimized the interacting complexes by means of the same PBE functional, in conjunction with a DZ basis set, as implemented in the SIESTA 3.0 program package.[61] The inner electronic shells were described through nonrelativistic pseudopotentials, whereas the I 5s5p, Cl 3s3p, O, N, and C 2s2p, H 1s, Ti 4s3d, and Pb 6s6p5d electrons were explicitly included in the calculations. A value of 100 Ry was used as the plane wave cutoff for the grid. Our model system was made of a $3 \times 5 \times 3$ pseudocubic perovskite slab exposing the 110 surfaces. The perovskite slab stoichiometry was $MA_{60}Pb_{45}I_{150}$, and thus, it deviated from the ideal material stoichiometry, in line with the analysis of perovskites surfaces by Mitzi.[62] By following the same approach as that reported in our previous studies,[54,63] we deposited the $3 \times 5 \times 3$ pseudocubic perovskite slab, exposing (110) surfaces onto a $5 \times 3 \times 2$ TiO_2 slab. The interaction of the $MAPbI_3$ perovskite with the TiO_2 surface mainly took place through binding of undercoordinated perovskite iodide atoms to undercoordinated titanium atoms of the TiO_2 surface. The experimental TiO_2 cell parameters (a = 18.92 Å and b = 30.72 Å) were employed to build a periodic supercell in the x and y directions, leaving 10 Å vacuum along the z direction. Electronic structure analyses were performed using the Quantum Espresso program package on the structures optimized by SIESTA. We previously checked that SIESTA and Quantum Espresso provide perfectly coherent results for the $MAPbI_3$ perovskite slab and for its interface with TiO_2.

Acknowledgements

The research leading to these results has received funding from the European Union Seventh Framework Programme [FP7/2007%2013] under Grant Agreement No. 604032 of the MESO project. JMA would like to thank Eusko Jaurlaritza (Basque Government) for funding through a postdoc fellowship. JB thanks financial support by MINECO of Spain (project MAT2013-47192-C3-1-R).

References

1 A. Kojima, K. Teshima, Y. Shirai and T. Miyasaka, *J. Am. Chem. Soc.*, 2009, **131**, 6050–6051.
2 J.-H. Im, C.-R. Lee, J.-W. Lee, S.-W. Park and N.-G. Park, *Nanoscale*, 2011, **3**, 4088–4093.
3 H.-S. Kim, C.-R. Lee, J.-H. Im, K.-B. Lee, T. Moehl, A. Marchioro, S.-J. Moon, R. Humphry-Baker, J.-H. Yum, J. E. Moser, M. Grätzel and N.-G. Park, *Sci. Rep.*, 2012, **2**, 591.
4 M. M. Lee, J. Teuscher, T. Miyasaka, T. N. Murakami and H. J. Snaith, *Science*, 2012, 338.
5 L. Etgar, P. Gao, Z. Xue, Q. Peng, A. K. Chandiran, B. Liu, M. K. Nazeeruddin and M. Grätzel, *J. Am. Chem. Soc.*, 2012, **134**, 17396–17399.
6 J. H. Noh, S. H. Im, J. H. Heo, T. N. Mandal and S. I. Seok, *Nano Lett.*, 2013, **13**, 1764–1769.
7 D. Zhong, B. Cai, X. Wang, Z. Yang, Y. Xing, S. Miao, W.-H. Zhang and C. Li, *Nano Energy*, 2015, **11**, 409–418.
8 M. Liu, M. B. Johnston and H. J. Snaith, *Nature*, 2013, **501**, 395–398.
9 N. J. Jeon, J. H. Noh, W. S. Yang, Y. C. Kim, S. Ryu, J. Seo and S. I. Seok, *Nature*, 2015, **517**, 476–480.
10 H. Zhou, Q. Chen, G. Li, G. Luo, T.-b. Song, H.-S. Duan, Z. Hong, J. You, Y. Liu and Y. Yang, *Science*, 2013, **345**, 542–546.
11 R. Gottesman, E. Haltzi, L. Gouda, S. Tirosh, Y. Bouhadana, A. Zaban, E. Mosconi and F. De Angelis, *J. Phys. Chem. Lett.*, 2014, **5**, 2662–2669.
12 E. J. Juarez-Perez, R. S. Sanchez, L. Badia, G. Garcia-Belmonte, Y. S. Kang, I. Mora-Sero and J. Bisquert, *J. Phys. Chem. Lett.*, 2014, **5**, 2390–2394.
13 H. J. Snaith, A. Abate, J. M. Ball, G. E. Eperon, T. Leijtens, N. K. Noel, S. D. Stranks, J. T.-W. Wang, K. Wojciechowski and W. Zhang, *J. Phys. Chem. Lett.*, 2014, **5**, 1511–1515.
14 H.-W. Chen, N. Sakai, M. Ikegami and T. Miyasaka, *J. Phys. Chem. Lett.*, 2015, **6**, 164–169.
15 W. Tress, N. Marinova, T. Moehl, S. M. Zakeeruddin, M. K. Nazeeruddin and M. Grätzel, *Energy Environ. Sci.*, 2015, **8**, 995–1004.
16 H.-S. Kim and N.-G. Park, *J. Phys. Chem. Lett.*, 2014, **5**, 2927–2934.
17 E. L. Unger, E. T. Hoke, C. D. Bailie, W. H. Nguyen, A. R. Bowring, T. Heumuller, M. G. Christoforo and M. D. McGehee, *Energy Environ. Sci.*, 2014, **7**, 3690–3698.
18 B. Chen, X. Zheng, M. Yang, Y. Zhou, S. Kundu, J. Shi, K. Zhu and S. Priya, *Nano Energy*, 2015, **13**, 582–591.
19 N.-G. Park, *Nat. Mater.*, 2014, **14**, 140–141.
20 Z. Xiao, Y. Yuan, Y. Shao, Q. Wang, Q. Dong, C. Bi, P. Sharma, A. Gruverman and J. Huang, *Nat. Mater.*, 2014, **14**, 193–198.
21 Y. Shao, Z. Xiao, C. Bi, Y. Yuan and J. Huang, *Nat. Commun.*, 2014, **5**, 5784.
22 K. Wojciechowski, S. D. Stranks, A. Abate, G. Sadoughi, A. Sadhanala, N. Kopidakis, G. Rumbles, C.-Z. Li, R. H. Friend, A. K.-Y. Jen and H. J. Snaith, *ACS Nano*, 2014, **8**, 12701–12709.
23 Z. Xiao, C. Bi, Y. Shao, Q. Dong, Q. Wang, Y. Yuan, C. Wang, Y. Gao and J. Huang, *Energy Environ. Sci.*, 2014, **7**, 2619–2623.
24 G. Xing, B. Wu, S. Chen, J. Chua, N. Yantara, S. Mhaisalkar, N. Mathews and T. C. Sum, *Small*, 2015, DOI: 10.1002/smll.201403719.
25 A. Marchioro, J. Teuscher, D. Friedrich, M. Kunst, R. van de Krol, T. Moehl, M. Grätzel and J.-E. Moser, *Nat. Photonics*, 2014, **8**, 250–255.

26 H. Nagaoka, F. Ma, D. W. deQuilettes, S. M. Vorpahl, M. S. Glaz, A. E. Colbert, M. E. Ziffer and D. S. Ginger, *J. Phys. Chem. Lett.*, 2015, **6**, 669–675.
27 L. Bertoluzzi, R. S. Sanchez, L. Liu, J.-W. Lee, E. Mas-Marza, H. Han, N.-G. Park, I. Mora-Sero and J. Bisquert, *Energy Environ. Sci.*, 2015, **8**, 910–915.
28 J. M. Frost, K. T. Butler and A. Walsh, *APL Mater.*, 2014, **2**, 081506.
29 Y. Kutes, L. Ye, Y. Zhou, S. Pang, B. D. Huey and N. P. Padture, *J. Phys. Chem. Lett.*, 2014, **5**, 3335–3339.
30 J. M. Frost, K. T. Butler, F. Brivio, C. H. Hendon, M. van Schilfgaarde and A. Walsh, *Nano Lett.*, 2014, **14**, 2584–2590.
31 J. Xu, A. Buin, A. H. Ip, W. Li, O. Voznyy, R. Comin, M. Yuan, S. Jeon, Z. Ning, J. J. McDowell, P. Kanjanaboos, J.-P. Sun, X. Lan, L. N. Quan, D. H. Kim, I. G. Hill, P. Maksymovych and E. H. Sargent, *Nat. Commun.*, 2015, **6**, 7081.
32 C. Quarti, E. Mosconi and F. De Angelis, *Chem. Mater.*, 2014, **26**, 6557–6569.
33 M. Coll, A. Gomez, E. Mas-Marza, O. Almora, G. Garcia-Belmonte, M. Campoy-Quiles and J. Bisquert, *J. Phys. Chem. Lett.*, 2015, **6**, 1408–1413.
34 J. Beilsten-Edmands, G. E. Eperon, R. D. Johnson, H. J. Snaith and P. G. Radaelli, *Appl. Phys. Lett.*, 2015, **106**, 173502.
35 B. C. O'Regan, P. R. F. Barnes, X. Li, C. Law, E. Palomares and J. M. Marin-Beloqui, *J. Am. Chem. Soc.*, 2015, **137**, 5087–5099.
36 M. S. Islam, *J. Mater. Chem.*, 2000, **10**, 1027–1038.
37 A. B. Mun, A. M. Ritzmann, M. Pavone, J. A. Keith and E. A. Carter, *Acc. Chem. Res.*, 2014, **47**, 3340–3348.
38 A. M. Ritzmann, A. B. Mun, M. Pavone, J. A. Keith and E. A. Carter, *Chem. Mater.*, 2013, **25**, 3011–3019.
39 A. M. Ritzmann, M. Pavone, A. B. Muñoz-García, J. A. Keith and E. A. Carter, *J. Mater. Chem. A*, 2014, **2**, 8060–8074.
40 J. Misuzaki, K. Arai and K. Fueki, *Solid State Ionics*, 1983, **11**, 203–211.
41 E. T. Hoke, D. J. Slotcavage, E. R. Dohner, A. R. Bowring, H. I. Karunadasa and M. D. McGehee, *Chem. Sci.*, 2014, **6**, 613–617.
42 M. L. Agiorgousis, Y.-Y. Sun, H. Zeng and S. Zhang, *J. Am. Chem. Soc.*, 2014, **136**, 14570–14575.
43 A. Buin, P. Pietsch, J. Xu, O. Voznyy, A. H. Ip, R. Comin and E. H. Sargent, *Nano Lett.*, 2014, **14**, 6281–6286.
44 M. H. Du, *J. Mater. Chem. A*, 2014, **2**, 9091–9098.
45 A. Walsh, D. O. Scanlon, S. Chen, X. G. Gong and S.-H. Wei, *Angew. Chem., Int. Ed.*, 2014, **53**, 1–5.
46 W.-J. Yin, T. Shi and Y. Yan, *Appl. Phys. Lett.*, 2014, **104**, 063903.
47 M. W. Ammann, J. P. Brodholt and D. P. Dobson, *Phys. Chem. Miner.*, 2008, **36**, 151–158.
48 M. Saiful Islam, *J. Mater. Chem.*, 2000, **10**, 1027–1038.
49 M.-H. Du, *J. Phys. Chem. Lett.*, 2015, **6**, 1461–1466.
50 O. Almora, I. Zarazua, E. Mas-Marza, I. Mora-Sero, J. Bisquert and G. Garcia-Belmonte, *J. Phys. Chem. Lett.*, 2015, **6**, 1645–1652.
51 E. Mosconi, E. Ronca and F. De Angelis, *J. Phys. Chem. Lett.*, 2014, **5**, 2619–2625.
52 F. Nunzi, E. Mosconi, L. Storchi, E. Ronca, A. Selloni, M. Grätzel and F. De Angelis, *Energy Environ. Sci.*, 2013, **6**, 1221–1229.
53 E. Mosconi, A. Amat, K. Nazeeruddin, M. Grätzel and F. De Angelis, *J. Phys. Chem. C*, 2013, 117.
54 V. Roiati, E. Mosconi, A. Listorti, S. Colella, G. Gigli and F. De Angelis, *Nano Lett.*, 2014, **14**, 2168–2174.
55 V. W. Bergmann, S. A. L. Weber, F. J. Ramos, M. K. Nazeeruddin, M. Grätzel, D. Li, A. L. Domanski, I. Lieberwirth and S. Ahmad, *Nat. Commun.*, 2014, 1–9.
56 E. Edri, S. Kirmayer, S. Mukhopadhyay, K. Gartsman, G. Hodes and D. Cahen, *Nat. Commun.*, 2014, 1–8.
57 A. L. Laban and L. Etgar, *Energy Environ. Sci.*, 2013, **6**, 3249–3252.
58 P. Giannozzi, S. Baroni, N. Bonini, M. Calandra, R. Car, C. Cavazzoni, D. Ceresoli, G. L. Chiarotti, M. Cococcioni, I. Dabo, A. D. Corso, S. de Gironcoli, S. Fabris, G. Frates, R. Gebauer, U. Gerstmann, C. Gougoussis, A. Kokalj, M. Lazzeri, L. Martin-Samos, N. Marzari, F. Mauri, R. Mazzarello, S. Paolini, A. Pasquarello, L. Paulatto, C. Sbraccia, S. Scandolo, G. Sclauzero, A. P. Seitsonen, A. Smogunov, P. Umari and R. M. Wentzcovitch, *J. Phys.: Condens. Matter*, 2009, **21**, 395502.
59 J. P. Perdew, K. Burke and M. Ernzerhof, *Phys. Rev. Lett.*, 1996, **77**, 3865–3868.
60 A. Poglitsch and D. Weber, *J. Chem. Phys.*, 1987, **87**, 6373–6378.
61 J. M. Soler, E. Artacho, J. D. Gale, A. García, J. Junquera, P. Ordejón and D. Sánchez-Portal, *J. Phys.: Condens. Matter*, 2002, **14**, 2745–2779.
62 D. B. Mitzi, *J. Mater. Chem.*, 2004, **14**, 2355–2365.
63 S. Colella, E. Mosconi, G. Pellegrino, A. Alberti, V. L. P. Guerra, S. Masi, A. Listorti, A. Rizzo, G. G. Condorelli, F. De Angelis and G. Gigli, *J. Phys. Chem. Lett.*, 2014, **5**, 3532–3538.